Active Targeting Nanotheranostic System for Dual-Modality Imaging-Guided Chemo-/Photodynamic Therapy of Pancreatic Cancer

Yong Han (hanrong2002@163.com)
Nantong University Affiliated Hospital: Affiliated Hospital of Nantong University
Qiusha Tang
Southeast University Medical College
Gang Jia
Henan Provincial People's Hospital
Yanli An
Southeast University Zhongda Hospital
Yinan Ding
Southeast University Medical College

Research

Keywords: Photodynamic therapy, Pancreatic cancer, Targeted therapy, Upconversion nanoparticles, Luminescence resonance energy transfer

Posted Date: May 18th, 2021

DOI: https://doi.org/10.21203/rs.3.rs-486069/v1

Abstract

Background: Pancreatic cancer (PC) is one of the most devastating types of cancers worldwide and has a remarkably poor survival rate, emphasizing the need for more effective strategies for the diagnosis and therapy of PC. Upconversion nanoparticles (UCNPs) have gained a privileged place in the biomedical field due to their outstanding properties. Besides, epithelial cell adhesion molecule (EpCAM) as one of the key biomarkers of pancreatic cancer stem cells, is a vital target for theranostic, diagnostic, and/or therapeutic intervention in nanomedicine. In this study, the theranostic nanosystem (EpCAM-UCMSNs-MX) was formed from the mesoporous silica-coated UCNPs functionalized with anti-EpCAM monoclonal antibody, and then one anticancer drug and photosensitizer, mitoxantrone (MX), was loaded into the mesoporous silica. The nanotheranostic system was used to target caner stem cells for realizing simultaneous dual-modality MR/UCL imaging and synergetic chemotherapy and NIR-triggered PDT.

Results: After conducting series of characterizations, the nanotheranostic systems own superior uniform sphericity and long-time stability. In vitro and vivo experiments show the nanocomposites have good biocompatibility and can target caner stem cells to realize simultaneous dual-modality MR/UCL imaging. Furthermore, in comparison with UCMSNs-MX and free MX, MX-loaded UCMSNs conjugated with anti-EpCAM monoclonal antibody (EpCAM-UCMSNs-MX) are efficiently endocytosed by cancerous cells and show synergetic effect with PDT in vitro. In vivo experiments reconfirm the synergistic effects observed with the combination of EpCAM-UCMSNs-MX and PDT, which results in better treatment outcomes as compared to chemotherapy or NIR irradiation alone that fail to show any noticeable systemic toxicity.

Conclusions: The resulting nanotheranostics were shown to target caner stem cells to confer simultaneous dual-modality MR/UCL imaging and induced intracellular reactive oxygen species exposed to 980 nm excitation, leading to synergetic chemotherapy and NIR-triggered PDT. These results offer a promising strategy for designing a multifunctional nanotheranostic system for dual-modality imaging-guided synergistic oncotherapy.

Introduction

Pancreatic cancer (PC) is one of the most intractable cancers and presents extremely limited treatment options, and the 5-year survival rate is below 5%[1]. Although surgical procedure is the preferred treatment for patients with PC, approximately 80% patients suffer from complications that are unmanageable with curative surgery[2]. Moreover, other forms of therapies, including chemotherapy, radiotherapy and immunotherapy, exhibit limited efficacies[3, 4], highlighting the need for the development of other therapeutic strategies.

Photodynamic therapy (PDT) has recently drawn extensive attention as a potential cancer treatment, owing to its noninvasive properties and negligible drug resistance[5]. Upon proper light irradiation, photosensitizers (PSs) may convert light energy into oxygen molecules, generating local cytotoxic reactive oxygen species (ROS) that ablate malignant cells[6]. Despite making important success for PDT,

significant challenges still exist such as poor cancerous endocytosis and insufficient therapeutic effect[7, 8]. In addition, the applications of PDT is restricted by its limited penetration depth, as many PSs are activated by visible or UV light[9]. Mitoxantrone (MX), a type of broad-spectrum antitumor drug, is known to have less systemic toxicity than other anthracycline antibiotics. MX has been studied in nanomedicine research[10–14]. Of note, in view of two major absorption peaks at 610 and 660 nm, MX may act as an efficient PS to kill cancer cells following irradiation at 660 nm wavelength[15]. In particular, MX has been verified as a remarkably efficient PS that mediates cell apoptosis and damage under light excitation.

In comparison with chemotherapy or PDT alone, the integration of chemotherapy and PDT has been shown to offer better therapeutic outcomes[16–20]. However, previous studies failed to show any in vivo results about introducing one reagent as anticancer drug and PS simultaneously or only studied the therapeutic effects of intratumorally injection or used a higher power density of laser, most importantly rare literature have been reported on active chemo-/PDT targeting pancreatic cancer stem cells[21–23]. It is common knowledge that epithelial cell adhesion molecule (EpCAM), as one of the key biomarkers of cancer stem cells (CSCs), involves the proliferation, differentiation, migration, and invasion of cancer. EpCAM is becoming a promising target for theranostic, diagnostic, and/or therapeutic intervention in nanomedicine. The use of MX coupled with EpCAM to allow MX release in CSCs may facilitate the release of adequate ROS, thereby resulting in cell apoptosis and death. However, the current nanosystems exhibit common drawbacks such as the laborious synthetic strategy, poor PS-loading ability, and lack of active CSCs-targeting superiority[24]. The construction of an active EpCAM-targeting drug delivery system that allows efficient loading and targeted delivery of MX is desirable.

Integrating diagnostic and therapeutic function into one nanoplatform, theranostic-oriented nanosystem may realize imaging and therapy simultaneously, thereby facilitating personalized medicine possible. Lanthanide ion-doped upconversion nanoparticles are deemed as dual-modality magnetic resonance/upconversion luminescent (MR/UCL) imaging probes, owing to their superior physicochemical properties[25, 26]. UCNPs-based combination chemotherapy and PDT were demonstrated to show superior treatment outcomes relative to single therapy modality.

Herein, we synthesized innovative active targeting nanoparticles (EpCAM-UCMSNs) by loading MX and used these for MR/UCL dual-modality imaging to investigate their active targeting abilities and therapeutic efficacies in vivo (Scheme 1). Our studies have demonstrated that the integration of PDT and chemotherapy may synergistically improve the efficiency of cancer therapy, which may be a good inception for the application of chemo-/PDT for the clinical treatment of PC.

Results And Discussion

Synthesis and characterizations

We synthesized $NaYF_4$:Yb,Er nanoparticles using a typical thermal decomposition according to our previous report[27]. As displayed in Fig. 1a, $NaYF_4$:Yb,Er nanoparticles were monodispersed with an

average size of 22.7 nm. Afterwards, a homogenous layer of $NaGdF_4$ was grown onto $NaYF_4$:Yb,Er nanoparticles. As showcased in Fig. 1b, the synthesized $NaYF_4$:Yb/Er@$NaGdF_4$ nanoparticles (UCNPs) displayed a uniform spherical morphology with an average size of 30.3 nm. TEM characterization (Fig. 1c) revealed the good dispersity of the synthesized UCMSNs. UCNPs exhibited a hexagonal phase (Fig. S1a), which is favorable for achieving highly luminescent and MR imaging probes. Furthermore, elements such as Na, F, Y, Yb, Er, and Gd in UCNPs were determined with energy-dispersive X-ray (EDX) spectroscopy (Fig. S1b). The photoluminescence intensity of UCNPs standardized based on the concentration of Y element increased by 3.5-fold relative to that of $NaYF_4$:Yb,Er nanoparticles; the emission intensity mostly contributed to the in vivo detection sensitivity (Fig. 2a). The surface modification of nanoparticles with mesoporous silica is known to enhance their biocompatibility and stability under physiological conditions. Furthermore, mesoporous silica may serve as an efficient drug reservoir and vehicle for encapsulating drugs[28–31]. With these advantages in mind, we converted the oil-phase OA-UCNPs in cyclohexane to an aqueous phase following treatment with a weak acid. CTAC was introduced as for the modification of mesoporous silica on ligand-free UCNPs, followed by the coating of mesoporous silica shell onto UCNPs as previously described[32].

EpCAM, as one important biomarker of CSCs in PC, has been established as the target for cancer therapy. Here, anti-EpCAM monoclonal antibody was covalently grafted onto the surface of UCMSNs based on esterification reaction, as confirmed by FTIR absorption spectra characterization. As indicated in Fig. 2b, the characteristic bands at 800-1,200 cm^{-1} for UCMSNs, UCMSNs-NH_2, and UCMSNs-EpCAM may be indexed to Si-O-Si stretching, while the broad band at 3,463.6 cm^{-1} corresponded to the stretching vibration of the amino group on UCMSN-NH_2. The C-H bands at approximately 2,900 cm^{-1} and C = O stretching bond at 1,458.0 and 1,377.2 cm^{-1} were correlated with the covalent bonding of anti-EpCAM monoclonal antibody on UCMSNs, thereby confirming the successful attachment of anti-EpCAM monoclonal antibody. Furthermore, both UCMSNs and UCMSNs-EpCAM showed a narrow size distribution in PBS; the hydrodynamic diameters of UCMSNs and UCMSNs-EpCAMs were 82.5 and 93.5 nm (Fig. 2c), respectively. Three kinds of nanoparticles were well dispersed in PBS, FBS, and DMEM cell medium for 28 days (Fig. S2). Thus, these particles were markedly stable under physiological conditions. The size range and high stability of these nanoparticles were appropriate for theranostic applications. Besides, the surface-associated Gd^{3+} endowed the $NaYF_4$:Yb,Er nanoparticles with enhanced MR properties. Especially, the molar relaxivity (r_1) of UCMSNs was 3.75 $mM^{-1}\cdot s^{-1}$ (Fig. 2d).

Drug release from UCMSNs-MX

An effective drug delivery system is the one that shows no reaction with the encapsulated drug while at the same time prevents the premature release of the drug. The sustainable release of the encapsulated compound will result in better therapeutic effects on tumors. As shown in Fig. S3, UCMSNs exhibited high BET surface area (290.1 m^2/g) and large pores (4.5 nm), which serve as useful properties for drug delivery. We investigated if MX, a widely used antitumor drug and PS, may be loaded into the mesopores of UCMSNs and observed a loading capacity of 23.6%. The in vitro release of MX from UCMSNs-MX was

estimated with the dialysis method. As observed from the release profile in Fig. S4, MX was released from UCMSNs at a relatively faster rate, which may speed up the drug accumulation in cancerous cells and increase the therapeutic effect. The most prominent feature is that MX may play the role of an antitumor drug and PS in antitumor therapy. The encapsulation of MX into the active EpCAM-targeting drug delivery system (UCMSNs-EpCAM) may allow its direct delivery into the cytoplasm, thereby resulting in enhanced synergetic effect of chemo-/PDT.

NIR-induced $^1O_2$ production of UCMSNs-MX

The generation of cytotoxic singlet oxygen in adequate level is important for the anticancer effect of PDT. The efficiency of $^1O_2$ production by MX-encapsulated UCMSNs following 980 nm laser irradiation was investigated based on a standard protocol. DPBF may react with $^1O_2$ irreversibly and induce a reduction in the intensity of DPBF absorption at 417 nm. Free MX, UCMSNs and MX-loaded UCMSNs were investigated respectively. As shown in Fig. 3a, no depletion of DPBF was observed in groups without NIR excitation, indicative of the absence of $^1O_2$ production. For free MX and UCMSNs without MX encapsulation, no sign of $^1O_2$ production was observed upon 980 nm laser irradiation. On the contrary, UCMSN-MX showed obvious consumption of DPBF under 980 nm laser illumination, indicative of the production of $^1O_2$. Furthermore, the production of $^1O_2$ increased over time, as more DPBF was consumed. In summary, cytotoxic $^1O_2$ may be effectively generated by MX-UCMSNs under NIR light excitation, thereby inducing NIR-activated PDT.

Toxicity evaluation

Before conducting biological experiments, the potential cytotoxicity of UCMSNs/UCMSNs-EpCAM was examined against BxPc-3 cells using CCK-8 assay. As displayed in Fig. 3b&c, no remarkable change was seen in the viability of cells following their incubation with higher concentration (1,000 μg/mL) of these particles for 24/48 h. The negligible cytotoxicity of UCMSNs/UCMSNs-EpCAM showcased their excellent in vitro biocompatibility, which is critical for their in vivo applications. These observations may be associated with the mesoporous silica modification on UCNPs in the form of a stabilizing layer, which decreases the leakage of possible toxic ions and the consequent systemic toxicity of nanoparticles.

Biosafety is one key consideration for biomaterials to translate into biomedical applications. Therefore, healthy mice were administrated with 150 μL physiological saline containing UCMSNs/UCMSNs-EpCAM (50 mg/mL) to study their in vivo short/long-term toxicity. The results of the complete blood chemistry assay (Fig. S5-6) showed that all serum biochemistry parameters were within the physiological range even at 30 days post-injection. Meanwhile, no remarkable weight loss was seen in mice treated with UCMSNs/UCMSNs-EpCAM or control (Fig. S7). Furthermore, no obvious injuries and pathological changes were reported in H&E-stained samples of major organs (Fig. S8), thereby demonstrating that the synthesized nanoparticles are safe for further applications.

Cellular uptake study

EpCAM is overexpressed on the cell membrane of many solid tumors, especially highly upregulated in virtually all epithelial carcinomas. On the other hand, its expression is almost absent in most normal cells, indicative of its potential role as a promising target for theranostic applications. The cellular internalization of UCMSNs/UCMSNs-EpCAM was analyzed using CLSM equipped with an external CW 980 nm laser source. The upconversion luminescence emission of UCNPs was used for in vitro uptake study. BxPc-3 cells were treated with UCMSNs (non-targeted), UCMSNs-EpCAM (targeted), or UCMSNs-EpCAM coupled with free anti-EpCAM monoclonal antibody (the blocking group). As displayed in Fig. 4, a much higher green signal was seen in cells treated with UCMSNs-EpCAM compared to those treated with UCMSNs, demonstrating that anti-EpCAM may remarkably improve the cellular internalization of nanoparticles through receptor-mediated endocytosis. These results confirm that the specific binding between EpCAM-UCMSNs and EpCAM on the membrane of cancerous cells is essential for the efficient targeting of UCMSNs-EpCAM.

Synergetic effect of Chemo-/PDT in vitro

Aside from its application as a dual-modality imaging probe, UCMSNs may be used for loading anticancer drug, owing to their unique mesoporous structure. We loaded MX into UCMSNs and evaluated the production of cytotoxic $^1O_2$ from UCMSN-EpCAM-MX in response to the synergetic effect of chemotherapy and PDT in vitro. As showcased in Fig. 5a, no cell death was observed exposed to NIR irradiation alone. Without laser illumination, cells treated with free MX and MX-loaded UCMSNs (UCMSNs-MX) at 2.5 μg/mL concentration for 24 h showed a survival rate of 12% and 15%, respectively. On the contrary, the percentage of cell death was higher in the group treated with EpCAM-UCMSNs-MX (22.5%) as compared with that treated with UCMSNs-MX (17.4%); the increased treatment efficacy of EpCAM-UCMSNs-MX over MX-UCMSNs was related to more cellular uptake of targeted UCMSNs via antigen–antibody-mediated endocytosis. However, neither MX-UCMSNs nor EpCAM-UCMSNs-MX showed any PDT effect due to no $^1O_2$ production. The viability of cells treated with pure MX with or without laser irradiation were 83.7% and 76.8%, respectively. Thus, no significant cell death was observed when treated with MX and NIR excitation. Upon NIR irradiation, cell death dramatically increased to 68.8% with MX-UCMSNs and 95.7% with EpCAM-UCMSNs-MX. This drastic difference may be associated with the gradual uptake of EpCAM-UCMSNs-MX in the cytoplasm of BxPc-3 cells through endocytosis as compared to the enhanced permeability and retention (EPR) effect observed for UCMSNs-MX. These results suggest that EpCAM-UCMSNs-MX exhibited superior therapeutic effects as compared to UCMSN-MX and free MX. EpCAM-UCMSNs-MX could accumulate in cancer cells through specific antigen–antibody-mediated endocytosis and release MX to show synergetic chemo-/PDT effect. The high-Z ions (such as Yb^{3+} and Gd^{3+}) may help to the process of photosensitization. Furthermore, EpCAM-UCMSNs-MX may be used for EpCAM-targeted dual-modality imaging and MX delivery to achieve synergetic chemot-/PDT effect.

It is known that PDT produces ROS and induces programmed cell death via the activation of apoptotic pathway, wherein protease caspase-3 plays a key role in apoptosis[33]. Caspase-3 is derived from the proteolytic cleavage of the dormant procaspase-3 in the cytosol during the process of apoptosis.

Caspase-9 is first activated, followed by the subsequent activation of the downstream caspase-3[34]. In addition, mitochondrial injuries may trigger the release of cytochrome c (cyt c) in the cytoplasm of cancer cells after a series of different treatments. The Bcl-2/Bax protein complex plays a critical role by maintaining the mitochondrial membrane permeability and may induce the expression of downstream caspase-3, which in turn mediates cell survival or death[35, 36]. To further explore if ROS can inhibit tumor cell growth and increase their sensitivity to PDT, BxPc-3 cells received eight different treatments as mentioned above. The expression level of proteins involved in the mitochondrial apoptosis pathway was measured by western blot analysis to evaluate the potential mechanism underlying chemo-/PDT-induced cell death. As shown in Fig. 5b, the expression levels of Bax, caspase-3, and caspase-9 substantially increased in the cells subjected to chemo-/PDT treatment as compared with the cells from control, UCMSNs-MX plus NIR irradiation, and EpCAM-UCMSNs-MX without NIR irradiation ($P < 0.05$) group, thereby indirectly verifying the best antitumor effects in vitro. Caspase-3 in the group treated with EpCAM-UCMSNs-MX with NIR irradiation was approximately 2.4-fold higher than that observed for the control group, further demonstrating the activation of caspase-3 during PDT process (Fig. 5c). The level of Bcl-2 was greatly downregulated in the group with chemo-/PDT as compared with MX group ($P < 0.05$, Fig. 5d). The chemo-/PDT group exhibited the best anticancer effect, suggesting that EpCAM-UCMSNs-MX plus NIR irradiation may remarkably modulate the expression of survival-related proteins and consequently induce cell death. Thus, MX combined with PDT may suppress cell growth and increase cell apoptosis through the upregulation of Bax, caspase-9, and caspase-3 and downregulation of Bcl-2 expression (Fig. 5e&f). Taken together, mitochondrial apoptosis induced by the synergetic effect of chemo-/PDT was thought to be the key mechanism underlying BxPc-3 cell death.

Dual-modality MR/UCL imaging in vivo

As mentioned before, UCNPs emit luminescence at 660 nm wavelength upon excitation at 980 nm wavelength and may serve as outstanding imaging probes in vivo. The in vivo tumor accumulation of UCMSNs was studied in BxPc-3 tumor-bearing mice. Mice were administrated with UCMSNs/EpCAM-UCMSNs intravenously, respectively. As shown in Fig. 6a, green luminescence was notably different for both non-targeted and targeted group. The signal intensity was much higher in mice administrated with EpCAM-UCMSNs than those with UCMSNs, emphasizing the superior in vivo targeting ability (Fig. 6b). In comparison to UCMSNs that owned passive tumor-targeting ability alone, anti-EpCAM-conjugated UCMSNs owned both active and passive targeting abilities, thus followed by reducing more accumulation even at 48 h. To evaluate the biodistribution of the nanoparticles, mice were euthanized after 48 h of administration, and the tumor and various organs were harvested to image ex vivo. As shown in Fig. S9, much accumulation of nanoparticles was seen in the liver and spleen; moreover, the excised tumors showed more uptake of targeted nanoparticles as compared with non-targeted ones. Although the active targeting ability of EpCAM-UCMSNs may be influenced by unspecific proteins in the tumor microenvironment, the efficient in vivo imaging results suggests that the nonspecific adsorption of plasma proteins, if any, would fall within a very narrow range. Taken together, our results demonstrate that EpCAM-UCMSNs may effectively target PC cells, which warrants further studies in the future.

To explore the active targeting ability of EpCAM-UCMSNs, the in vivo MR scans were conducted before and after the intravenous injection with UCMSNs/EpCAM-UCMSN. Anti-EpCAM monoclonal antibody was grafted onto UCMSNs to allow binding to EpCAM overexpressed on CSCs of PC. As shown in Fig. 6c&d, MR imaging signal intensity increased by about 20.1% and 40.8% in BxPc-3 tumors treated with non-targeted and targeted nanoparticles, respectively, after 4 h of injection. This observation confirms that UCMSNs/EpCAM-UCMSNs were largely delivered to the tumor sites via active/passive targeting capabilities, which increased the signal intensity in MR imaging. Therefore, UCMSNs-EpCAM may be involved into one promising MR contrast specific to tumor sites.

In vivo synergetic chemo-/PDT

The above in vitro results of satisfactory dual-modality imaging and synergetic therapeutic efficacy encouraged us to investigate the therapeutic efficacies of UCMSNs-MX in vivo. When tumors of mice were palpable, they received the above treatments as mentioned above. Changes in relative tumor volume are shown in Fig. 7a. Mice treated with EpCAM-UCMSNs-MX showed better anticancer response than those treated with UCMSNs-MX ($P < 0.05$), demonstrating the superiority of active targeted drug delivery system. Moreover, the group treated with EpCAMs-UCMSNs-MX + NIR exhibited better results than that treated with EpCAM-UCMSNs-MX ($P < 0.01$), owing to the synergetic effect of MX-based chemotherapy and PDT triggered by NIR irradiation. The mice exposed to NIR illumination alone failed to show any therapeutic effect as compared with the control group. Furthermore, EpCAM-UCMSNs-MX + NIR group displayed remarkably significant delay in the tumor growth as compared with UCMSNs-MXs + NIR group ($P < 0.05$), as more EpCAM-UCMSNs-MX accumulated at the tumor sites and thus more MX was leaked in the tumor cells that contributed to the synergetic effect of chemo-/PDT. Final tumor volumes are summarized in Fig. S10. Tumors treated with EpCAM-UCMSNs-MX + NIR demonstrated maximum necrosis, as observed by images of H&E-stained tumor slices, which highlight the enhanced anticancer effect of the combination of chemotherapy and PDT as compared with other therapy types (Fig. S11). Meanwhile, no significant weight losses were observed in mice treated with EpCAM-UCMSNs-MX + NIR and EpCAM-UCMSNs-MX; a decrease in the body weight of mice treated with NS or NIR alone was observed over time, possibly attributed to the tumor progression and dyscrasia (Fig. 7b). Especially, mice from the chemo-/PDT group showed a remarkable increase in the survival period ($P < 0.05$, Fig. 7c). In brief, these results suggest that EpCAM-UCMSNs-MX based chemo-/PDT is an effective therapeutic strategy for the treatment of PC.

Biodistribution and targeting efficiency

To further evaluate active targeting efficiency of the EpCAM-UCMSNs/UCMSNs, the concentrations of Y^{3+} in the collected tumor and major organs were investigated based on ICP-MS analysis. As shown in Fig. 8, the nanoparticles primarily accumulated in the liver and spleen 12 h post-injection, confirming that the UCNPs-based nanocomposites could accumulate in the organs of the reticuloendothelial system. EpCAM-UCMSNs gradually increased 24 and 48 h post-injection and reached a peak higher than that of UCMSNs. This remarkably difference was attributed to active targeting ability due to anti-EpCAM-mediated

endocytosis. However, the contents of Y^{3+} stepped dowm in the tumors and major organs at 48 h post-injection, and this is due to slow clearance of the nanoparticles through a hepatobiliary route to a large extent. In addition, the targeting efficiencies of the above nanocomposites are statistically different at 24/48 h post-injection, respectively ($P < 0.05$). These results reconfirm the excellent active targeting ability of the EpCAM-UCMSNs.

Conclusions

We report the development of a potent theranostic nanosystem based on the combination of UCNPs and MX, which may be used for the dual-modality MR/UCL imaging-guided synergetic chemo-/PDT. The nanotheranostic system acts as a vehicle for the anticancer drug/PS (MX) and displays synergetic chemo-/PDT effect with the simultaneous MR/UCL dual-modality imaging. UCMSNs display excellent water dispersity and biocompatibility. In comparison with UCMSNs-MX and free MX, MX-loaded UCMSNs conjugated with anti-EpCAM monoclonal antibody (EpCAM-UCMSNs-MX) are efficiently endocytosed by cancerous cells and show synergetic effect with PDT in vitro. In vivo experiments reconfirm the synergistic effects observed with the combination of EpCAM-UCMSNs-MX and PDT, which results in better treatment outcomes as compared to chemotherapy or NIR irradiation alone that fail to show any noticeable systemic toxicity. Thus, UCNPs-based nanotheranostics may serve as a promising nanoplatform for future translational research in PC diagnosis and therapy. The multifunctional UCMSNs-based theranostics may be used with multiple types of sensitizers (radiosensitizers, thermosensitizers, and sonosensitizers) for malignant tumor treatment under simultaneous imaging guidance.

Experimental Section

Materials

Yttrium chloride hexahydrate ($YCl_3 \cdot 6H_2O$, 99.9%), gadolinium chloride hexahydrate ($GdCl_3 \cdot 6H_2O$, 99.9%), ytterbium chloride hexahydrate ($YbCl_3 \cdot 6H_2O$, 99.9%), erbium chloride hexahydrate ($ErCl_3 \cdot 6H_2O$, 99.9%), oleic acid (OA, 95%), 1-(3-dimethylaminopropyl)-3-ethylcarbodiimide hydrochloride (EDC), ammonium fluoride (NH_4F), 1-octadecene (ODE, 90%), N-hydroxysuccinimide (NHS), cetyltrimethylammonium chloride solution (CTAC), 3-aminopropyltrimethoxysilane (APTES, 98%), and 4,6-diamidino-2-phenylindole dihydrochloride (DAPI) were purchased from Sigma-Aldrich (Sydney, Australia). 2-(N-Morpholino) ethanesulfonic acid (MES, 99.0%) were obtained from Sinopharm Chemical Reagent Co., Ltd, Shanghai, China. Tetraethyl orthosilicate (TEOS) sodium chloride (NaCl), triethanolamine (TEA), methanol, and sodium hydroxide (NaOH) were purchased from Lingfeng Chemical Reagent Company (Shanghai, China). Anti-EpCAM monoclonal antibody was supplied by eBioscience (Austria). MX was procured from Toronto Research Chemicals Inc (Canada). Cell counting kit-8 (CCK-8) was purchased from Dojindo (Tokyo, Japan). All reagents were used as received unless otherwise stated.

Synthesis of UCNPs

$NaYF_4$:Yb,Er and $NaYF_4$:Yb,Er@$NaGdF_4$ nanoparticles (UCNPs) was synthesized using a typical thermal decomposition as described in our previous study[27].

Synthesis of UCNPs@mSiO $_2$ nanoparticles (UCMSNs) and UCMSNs-EpCAM

Cyclohexane solution of OA-UCNPs (50 mM, 2.5 mL) was added into 10 mL diluted hydrochloric acid (pH 4.0) and then stirred for 2 h. The products were under centrifugation, rinsed thrice with deionized water, and finally dispersed in 20 mL deionized water. TEA (0.01 g) and CTAC (0.5 g) were added and vigorously stirred for 2 h. A total of 10 mL ligand-free UCNPs solution was then added slowly, and the mixture was sonicated for 1 h. A total of 200 µL TEOS was added dropwise into the system and stirred vigorously at 80°C for 1 h. The obtained UCNPs@$mSiO_2$ nanoparticles (denoted as UCMSNs) were precipitated, washed thrice with ethanol, and extracted with 30 mL methanol solution of NaCl (1 wt %) at 25°C for 3 h to clear off the excess CTAC. After several cycles of extraction, UCMSNs were dispersed in deionized water for further use.

Anti-EpCAM monoclonal antibody was conjugated onto the surface of UCMSNs via an EDC/NHS coupling chemistry. Briefly, 50 µg anti-EpCAM monoclonal antibody in 10 mL MES buffer (pH: 6.0, 0.1 M) was reacted with equimolar ratio of EDC and NHS at 25°C for 15 min. Following incubation, UCMSNs-NH_2 nanoparticles dispersed in 100 mL phosphate-buffered saline (PBS, pH 8.5) were added to the above mixture and the system was performed for 2 h at 25°C. The resulting UCMSNs-EpCAM nanoparticles were centrifuged thrice with PBS to remove the unbound antibody and the final product was dispersed in 0.5 mL deionized water for use in subsequent experiments.

Characterization instruments

The morphologies of the above nanoparticles were studied using JEOL JEM-1200EX transmission electron microscope (TEM, Japan), while the size distribution study was performed using Image J software. Hydrodynamic diameters of UCMSNs and UCMSNs-EpCAM were measured with a Zeta-Plus analyzer (Brookhaven Instruments Co., Holtsville, USA). The concentrations of Y^{3+} element in the samples were estimated by an inductively coupled plasma mass spectrometry (ICP-MS, Jiangsu Skyray Instrument Co., China). The infrared spectra were acquired by a Fourier transform infrared (FTIR) spectrometer (Nicolet Co., USA). The concentration of MX was measured with ultraviolet-visible (UV-vis) spectrophotometry at a detection wavelength of 410 nm. Confocal laser scanning microscopic experiments were performed with Olympus FV1000 laser-scanning microscopy (Nikon, Japan) equipped with a continuous-wave NIR laser (λ = 980 nm) as the excitation source.

T_1-weighted MR properties of UCMSNs

Magnetic resonance properties of UCMSNs were evaluated with a 7.0 T MR scanner (Pharma Scan, Brukers, Germany). T_1 relaxation times depend on a multi-echo spin-echo sequence (16 echoes; repetition

time [TR] = 2,500 ms; echo time [TE] = 22–352 ms). T_1-weighted MR images of seven samples with gradient concentrations of Gd^{3+} (0, 4.33, 8.67, 17.35, 34.68, 69.30, and 138.56 μmol/mL) were acquired, and T_1 values were analyzed by measuring the signal intensity in 0.5 cm^2 region of interest. The relaxivity coefficient (r_1) was acquired as the gradient of the plot of R_1 ($R_1 = 1/T_1$) versus the molarity of magnetic atoms.

In vitro drug release of MX-UCMSNs

For in vitro studies, a total of 10 mL methanol solution containing 5 mg MX and 10 mg UCMSNs was stirred for 24 h at 25°C under dark condition. MX-UCMSNs product were gathered by centrifugation and freeze-dried under vacuum. The initial system and the supernatant were examined with a UV-vis spectrophotometry at 660 nm wavelength to analyze the concentration of MX in the above samples. The loading efficiency of MX in UCMSNs was measured using the formula: $(M_i - M_r)/M_i \times 100\%$; where, M_i: initial mass of MX and M_r: residual mass of MX after loading. To assess the drug-releasing characteristics of MX-UCMSNs, 5 mg pre-dried MX-UCMSNs were encapsulated into a dialysis bag (with 3,500 molecular weight cut-off) and placed in 20 mL PBS. Dialysis was performed in a table concentrator with a speed of 200 rpm at 25°C. At designated time-points, 3 mL solution was sampled as to examine the released MX mass and poured back in the initial dialysis medium. The total dialysis time was approximately 48 h.

In vitro toxicity assessment of UCMSNs/UCMSNs-EpCAM

Human PC cell line BxPc-3 were planted in a 96-well plate (2000 / well) overnight. The cells were incubated with UCMSNs/UCMSNs-EpCAM at different concentrations (3, 7.5, 15, 30, 60, 120, 250, 500, and 1000 μg/mL) in Dulbecco's modified Eagle's medium (DMEM) for 24/48 h. The cells were rinsed thrice with sterile PBS and co-incubated with 100 μL DMEM including 10 μL CCK-8 solution for 4 h. The absorbance values were measured at 450 nm. Cell survival percentage was the ratio of the absorbance of CCK-8 in the treated cells to that in the controls.

NIR-induced ROS generation in vitro

The intracellular ROS generation was determined with an oxidation sensitive fluorescent probe 1,3-diphenylisobenzofuran (DPBF)[28]. Briefly, 3000 BxPc-3 cells were cultured into a 96-well plate overnight, then were rinsed with sterile PBS and incubated with DMEM containing EpCAM-UCMSNs-MX/UCMSNs-MX (300 μg/mL) for 4 h. After incubation, the medium was removed and the cells were incubated with 100 μL DPBF for 1 h, then the cells were rinsed with PBS three times and illuminated with 980 nm light (320 mW/cm^2) for 10 min. The production of ROS was fluorometrically determined by examining the amount of DPBF and comparing it with the predetermined DPBF standard curve.

Cellular uptake study and targeting efficiency of UCMSNs/UCMSNs-EpCAM

BxPc-3 cells were cultured in confocal laser scanning microscopy (CLSM) special cell culture dish under a humidified 5% CO_2 atmosphere at 37°C. After reaching about 80% confluence, the cells were rinsed thrice with PBS. Following washing, the cells were treated with DMEM solution containing UCMSNs (200 μg/mL) and UCMSNs-EpCAM (200 μg/mL), respectively. After 4 h co-incubation, cells were gently rinsed with PBS three times and DAPI (1:1000) were used to stain the cell nuclei for 15 min. The excitation wavelength used was 980 nm.

In vivo toxicology study of UCMSNs/UCMSNs-EpCAM

Healthy female athymic nude mice (weight: 20 g, 5 weeks old) were purchased from the Model Animal Research Center of Nanjing University and raised at Laboratory Animal Center of Southeast University. All animal experimental procedures were approved by the Institutional Animal Care Committee at Southeast University. Mice were randomly divided into three groups as follows (six mice per cohort): two groups were administrated with a single dose of UCMSNs/UCMSNs-EpCAM in physiological saline (30 mg/mL, 150 μL) intravenously via tail vein. The third group was administrated with only 150 μL physiological saline and used as the control. Before blood collection, mice were anesthetized after 7 and 30 days of treatment and blood samples (approximately 500 μL) were acquired through cardiac puncture for biochemistry assays. All mice were euthanized and the major organs (heart, liver, spleen, lung, and kidney) were excised and fixed in a 10% formalin solution, followed by hematoxylin and eosin (H&E) staining.

Synergetic effect of chemo-/PDT in vitro

A total of 10^5 BxPc-3 cells were planted in a six-well plate and incubated overnight. After 80% confluence, the cells were rinsed with sterile PBS three times, then divided into eight groups and treated as follows: (1) PBS (50 μL), (2) PBS plus NIR irradiation, (3) MX, (4) MX and NIR irradiation, (5) UCMSNs-MX solution, (6) EpCAM-UCMSNs-MX solution, (7) UCMSNs-MX solution and 980 nm laser excitation, (8) EpCAM-UCMSNs-MX solution and 980 nm laser excitation. Briefly, 1 mL DMEM with MX/UCMSNs-MX/EpCAM-UCMSNs-MX ([MX] = 0.5 μg/mL) was added into the wells, and the cells were irradiated with 980 nm laser (320 mW/cm^2) for 5 min and then cultured for another 24 h. Cell viability was evaluated as described in Section ‘In vitro toxicity assessment of UCMSNs/UCMSNs-EpCAM’.

In vivo UCL imaging

To establish BxPc-3 tumor-bearing mice model, 2×10^6 cells were subcutaneously inoculated into right front flank of female balb/c nude mice. When the average volume of tumor reached approximately 80 mm^3, 10 mice were divided into two groups (five per group) randomly, two groups were then administrated intravenously with 150 μL of either UCMSNs (non-targeted group) or EpCAM-UCMSNs (targeted group) at a concentration of 20 mg/mL via tail vein. In vivo UCL images were recorded based on in vivo optical imaging system (Maestro EX, Cri, USA) at different time intervals (pre-injection and 1, 4, 8, 24, and 48 h post-injection). As an external source, a 0–10 W adjustable 980 nm laser was enrolled with a beam size of 30 mm, larger than the size of the tumor. Fluorescence intensities were determined at

different time points. Mice were euthanized at 48 h after treatment and the mean fluorescence intensities (MFI) of tumors and major organs were calculated.

In vivo MR imaging

BxPc-3 tumor-bearing mice model was established as described above. When the average volume of tumors was approximately 80 mm^3, MR scans were conducted using a 7.0 T Micro-MR imaging instrument (PharmaScan, Brukers, Germany). MR images were recorded at different time intervals such as at pre-injection and 1, 4, 8, 24, and 48 h post-injection (150 μL, 20 mg/mL). MR signal intensities were analyzed at each time point.

In vivo therapeutic effect of chemo-/PDT

BxPc-3 tumor-bearing mice with a uniform tumor size were grouped for in vivo treatment therapies. When the tumors reached an average diameter of 5–6 mm, ninety mice were divided into six groups. Group 1 only received 150 μL physiological saline alone intravenously via tail vein; group 2 received 150 μL physiological saline and NIR irradiation; group 3 received only 150 μL physiological saline containing UCMSNs-MX (12 mg/mL); group 4 was injected with 150 μL physiological saline containing EpCAM-UCMSNs-MX (12 mg/mL); group 5 received UCMSNs-MX intravenously and NIR irradiation; group 6 was injected with EpCAM-UCMSNs-MX (12 mg/mL, 150 μL) followed by NIR irradiation. For all NIR irradiation groups, a continuous-wave fiber-coupled 980 nm laser (320 mW/cm^2, 30 min, 5 min interval after every 5 min of irradiation) was applied at the tumor sites 8 h post-injection. All mice were administrated with two injections one week. Tumor volumes were measured with a digital caliper and calculated according to the formula $V = (width^2 \times length)/2$, and the weights of the mice were recorded every other day for 31 days. To further evaluate the treatment efficacy, the tumors and major organs were collected for H&E staining. The representative photos of tumors were recorded, respectively. Seven mice from each group were used for analyzing survival time.

Biodistribution and targeting efficiency

As mentioned above, BxPc-3 tumor-bearing mice were administrated with EpCAM-UCMSNs/UCMSNs (15 mg/mL, 150 μL, 5 mice per group) via tail vein, and euthanized at 12, 24, and 48 h post-injection. The contents of Y^{3+} in the tumor and major organs were measured based on ICP-MS. In addition, the targeting efficiency was evaluated as follows: targeting efficiency (%) = (total content of Y^{3+} in the sample/total content Y^{3+} in the injected nanoparticles) × 100%.

Statistics analysis

All the obtained data were analyzed using GraphPad Prism software (version 5.0). Differences between two groups was regarded as statistically significance for $*P < 0.05$ and very significant for $**P < 0.01$ and $***P < 0.001$.

Declarations

Acknowledgements

Not applicable.

Authors' contributions

YH, preparation and characterization of the UCNP-based nanotheranostics, carried out and analyzed the in vitro and animal experiments and the manuscript writing. QT, conceived the research and revised the manuscript. GJ, carried out animal experiments. YA, carried out and analyzed the in vitro experiments and manuscript revision. YD, made contributions to the analysis of the uptake studies and in the interpretation of the data. All authors read and approved the final manuscript.

Funding

The authors gratefully acknowledge funding support from the National Natural Science Foundation of China (81271635, 81301270), China Postdoctoral Science Foundation (2019M661908), and Doctoral Scientific Research Foundation of Affiliated Hospital of Nantong University (Tdb19017).

Availability of data and materials

The datasets used and/or analyzed during the current study are available from the corresponding author on reasonable request.

Ethical approval and consent to participate

All experiments in the research were conducted under a protocol approved by the Institutional Animal Care and Use Committee at Southeast University, China.

Consent for publication

Not applicable.

Competing interests

The authors have declared that no competing interest exists.

Author details

[1]Department of Radiation Oncology, Affiliated Hospital of Nantong University, Nantong, China. [2]Medical School of Southeast University, Nanjing, China. [3]Oncology Department of Henan Provincial People's Hospital, Zhengzhou, China. [4]Jiangsu Key Laboratory of Molecular and Functional Imaging, Department of Radiology, Zhongda Hospital, Medical School of Southeast University, Nanjing, China.

References

1. Siegel RL, Miller KD, Jemal A: **Cancer statistics, 2019.** *CA Cancer J Clin* 2019, **69:**7-34.
2. Spadi R, Brusa F, Ponzetti A, Chiappino I, Birocco N, Ciuffreda L, Satolli MA: **Current therapeutic strategies for advanced pancreatic cancer: A review for clinicians.** *World J Clin Oncol* 2016, **7:**27-43.

3. Huang L, Wei G, Sun X, Jiang Y, Huang Z, Huang Y, Shen Y, Xu X, Liao Y, Zhao C: **A tumor-targeted Ganetespib-zinc phthalocyanine conjugate for synergistic chemo-photodynamic therapy.** *Eur J Med Chem* 2018, **151:**294-303.
4. Shi H, Lu X, Liu Y, Song J, Deng K, Zeng Q, Wang C: **Nanotribological Study of Supramolecular Template Networks Induced by Hydrogen Bonds and van der Waals Forces.** *ACS Nano* 2018, **12:**8781-8790.
5. Idris NM, Gnanasammandhan MK, Zhang J, Ho PC, Mahendran R, Zhang Y: **In vivo photodynamic therapy using upconversion nanoparticles as remote-controlled nanotransducers.** *Nat Med* 2012, **18:**1580-1585.
6. Niedre M, Patterson MS, Wilson BC: **Direct near-infrared luminescence detection of singlet oxygen generated by photodynamic therapy in cells in vitro and tissues in vivo.** *Photochem Photobiol* 2002, **75:**382-391.
7. Pei Q, Hu X, Zheng X, Liu S, Li Y, Jing X, Xie Z: **Light-Activatable Red Blood Cell Membrane-Camouflaged Dimeric Prodrug Nanoparticles for Synergistic Photodynamic/Chemotherapy.** *ACS Nano* 2018, **12:**1630-1641.
8. Zhang L, Lei J, Ma F, Ling P, Liu J, Ju H: **A porphyrin photosensitized metal-organic framework for cancer cell apoptosis and caspase responsive theranostics.** *Chem Commun (Camb)* 2015, **51:**10831-10834.
9. Cui S, Yin D, Chen Y, Di Y, Chen H, Ma Y, Achilefu S, Gu Y: **In vivo targeted deep-tissue photodynamic therapy based on near-infrared light triggered upconversion nanoconstruct.** *ACS Nano* 2013, **7:**676-688.
10. Yao C, Li Y, Wang Z, Song C, Hu X, Liu S: **Cytosolic NQO1 Enzyme-Activated Near-Infrared Fluorescence Imaging and Photodynamic Therapy with Polymeric Vesicles.** *ACS Nano* 2020, **14:**1919-1935.
11. Li Z, Cai Y, Zhao Y, Yu H, Zhou H, Chen M: **Polymeric mixed micelles loaded mitoxantrone for overcoming multidrug resistance in breast cancer via photodynamic therapy.** *Int J Nanomedicine* 2017, **12:**6595-6604.
12. Li X, Yu S, Lee D, Kim G, Lee B, Cho Y, Zheng BY, Ke MR, Huang JD, Nam KT, et al: **Facile Supramolecular Approach to Nucleic-Acid-Driven Activatable Nanotheranostics That Overcome Drawbacks of Photodynamic Therapy.** *ACS Nano* 2018, **12:**681-688.
13. Bakhshizadeh M, Sazgarnia A, Seifi M, Hadizadeh F, Rajabzadeh G, Mohajeri SA: **TiO2-based Mitoxantrone Imprinted Poly (Methacrylic acid-co-polycaprolctone diacrylate) Nanoparticles as a Drug Delivery System.** *Curr Pharm Des* 2017, **23:**2685-2694.
14. Li Z, Zhang FL, Pan LL, Zhu XL, Zhang ZZ: **Preparation and characterization of injectable Mitoxantrone poly (lactic acid)/fullerene implants for in vivo chemo-photodynamic therapy.** *J Photochem Photobiol B* 2015, **149:**51-57.
15. Cai XJ, Li WM, Zhang LY, Wang XW, Luo RC, Li LB: **Photodynamic therapy for intractable bronchial lung cancer.** *Photodiagnosis Photodyn Ther* 2013, **10:**672-676.

16. Hou Z, Deng K, Li C, Deng X, Lian H, Cheng Z, Jin D, Lin J: **808 nm Light-triggered and hyaluronic acid-targeted dual-photosensitizers nanoplatform by fully utilizing Nd(3+)-sensitized upconversion emission with enhanced anti-tumor efficacy.** *Biomaterials* 2016, **101:**32-46.
17. Liang L, Lu Y, Zhang R, Care A, Ortega TA, Deyev SM, Qian Y, Zvyagin AV: **Deep-penetrating photodynamic therapy with KillerRed mediated by upconversion nanoparticles.** *Acta Biomater* 2017, **51:**461-470.
18. Zhang X, Ai F, Sun T, Wang F, Zhu G: **Multimodal Upconversion Nanoplatform with a Mitochondria-Targeted Property for Improved Photodynamic Therapy of Cancer Cells.** *Inorg Chem* 2016, **55:**3872-3880.
19. Lucky SS, Idris NM, Huang K, Kim J, Li Z, Thong PS, Xu R, Soo KC, Zhang Y: **In vivo Biocompatibility, Biodistribution and Therapeutic Efficiency of Titania Coated Upconversion Nanoparticles for Photodynamic Therapy of Solid Oral Cancers.** *Theranostics* 2016, **6:**1844-1865.
20. Hu J, Luo H, Qu Q, Liao X, Huang C, Chen J, Cai Z, Bao Y, Chen G, Li B, Cui W: **Cell Membrane-Inspired Polymeric Vesicles for Combined Photothermal and Photodynamic Prostate Cancer Therapy.** *ACS Appl Mater Interfaces* 2020.
21. Dai L, Yu Y, Luo Z, Li M, Chen W, Shen X, Chen F, Sun Q, Zhang Q, Gu H, Cai K: **Photosensitizer enhanced disassembly of amphiphilic micelle for ROS-response targeted tumor therapy in vivo.** *Biomaterials* 2016, **104:**1-17.
22. Yamagishi K, Kirino I, Takahashi I, Amano H, Takeoka S, Morimoto Y, Fujie T: **Tissue-adhesive wirelessly powered optoelectronic device for metronomic photodynamic cancer therapy.** *Nat Biomed Eng* 2019, **3:**27-36.
23. Guan Y, Lu H, Li W, Zheng Y, Jiang Z, Zou J, Gao H: **Near-Infrared Triggered Upconversion Polymeric Nanoparticles Based on Aggregation-Induced Emission and Mitochondria Targeting for Photodynamic Cancer Therapy.** *ACS Appl Mater Interfaces* 2017, **9:**26731-26739.
24. Yuan Y, Zhang CJ, Liu B: **A platinum prodrug conjugated with a photosensitizer with aggregation-induced emission (AIE) characteristics for drug activation monitoring and combinatorial photodynamic-chemotherapy against cisplatin resistant cancer cells.** *Chem Commun (Camb)* 2015, **51:**8626-8629.
25. Ai F, Sun T, Xu Z, Wang Z, Kong W, To MW, Wang F, Zhu G: **An upconversion nanoplatform for simultaneous photodynamic therapy and Pt chemotherapy to combat cisplatin resistance.** *Dalton Trans* 2016, **45:**13052-13060.
26. Oliani WL, Parra DF, Komatsu LGH, Lincopan N, Rangari VK, Lugao AB: **Fabrication of polypropylene/silver nanocomposites for biocidal applications.** *Mater Sci Eng C Mater Biol Appl* 2017, **75:**845-853.
27. Winkler HC, Notter T, Meyer U, Naegeli H: **Critical review of the safety assessment of titanium dioxide additives in food.** *J Nanobiotechnology* 2018, **16:**51.
28. Liu JN, Bu WB, Shi JL: **Silica coated upconversion nanoparticles: a versatile platform for the development of efficient theranostics.** *Acc Chem Res* 2015, **48:**1797-1805.

29. Yang D, Ma P, Hou Z, Cheng Z, Li C, Lin J: **Current advances in lanthanide ion (Ln(3+))-based upconversion nanomaterials for drug delivery.** *Chem Soc Rev* 2015, **44:**1416-1448.
30. Shiekh PA, Singh A, Kumar A: **Engineering Bioinspired Antioxidant Materials Promoting Cardiomyocyte Functionality and Maturation for Tissue Engineering Application.** *ACS Appl Mater Interfaces* 2018, **10:**3260-3273.
31. Shi J, Sun X, Zheng S, Li J, Fu X, Zhang H: **A new near-infrared persistent luminescence nanoparticle as a multifunctional nanoplatform for multimodal imaging and cancer therapy.** *Biomaterials* 2018, **152:**15-23.
32. Fan W, Shen B, Bu W, Zheng X, He Q, Cui Z, Zhao K, Zhang S, Shi J: **Design of an intelligent sub-50 nm nuclear-targeting nanotheranostic system for imaging guided intranuclear radiosensitization.** *Chem Sci* 2015, **6:**1747-1753.
33. Zhao N, Wu B, Hu X, Xing D: **NIR-triggered high-efficient photodynamic and chemo-cascade therapy using caspase-3 responsive functionalized upconversion nanoparticles.** *Biomaterials* 2017, **141:**40-49.
34. Du ZJ, Cui GQ, Zhang J, Liu XM, Zhang ZH, Jia Q, Ng JC, Peng C, Bo CX, Shao H: **Inhibition of gap junction intercellular communication is involved in silica nanoparticles-induced H9c2 cardiomyocytes apoptosis via the mitochondrial pathway.** *Int J Nanomedicine* 2017, **12:**2179-2188.
35. Ashkenazi A, Fairbrother WJ, Leverson JD, Souers AJ: **From basic apoptosis discoveries to advanced selective BCL-2 family inhibitors.** *Nat Rev Drug Discov* 2017, **16:**273-284.
36. Martinou JC, Youle RJ: **Mitochondria in apoptosis: Bcl-2 family members and mitochondrial dynamics.** *Dev Cell* 2011, **21:**92-101.

Figures

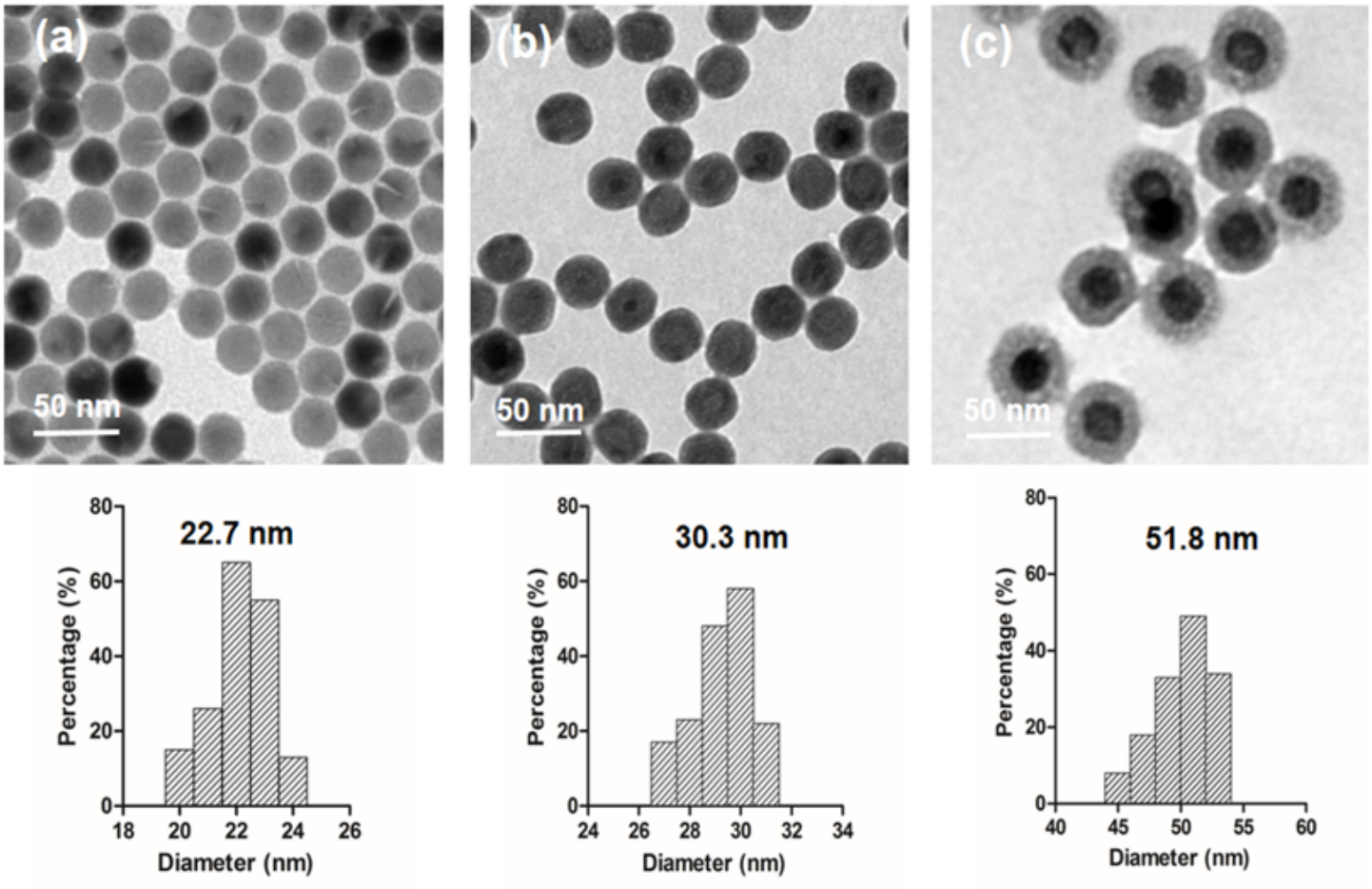

Figure 1

TEM images and size histograms of NaYF4:Yb,Er (a), NaYF4: Yb,Er@NaGdF4 (UCNPs, b) and UCNP@mSiO2 (UCMSNs, c).

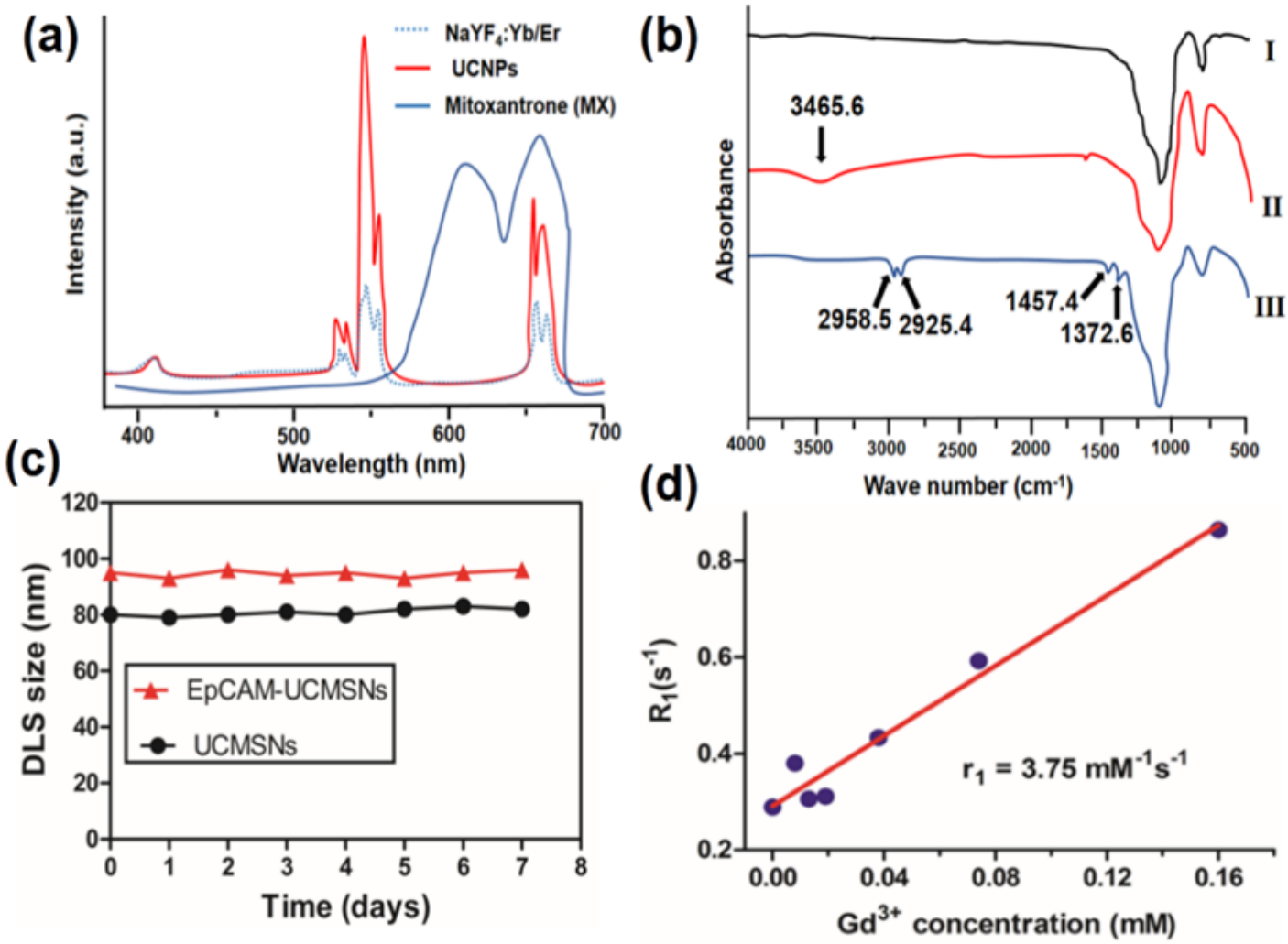

Figure 2

(a) Spectral overlap between the upconversion emission spectrum of the NaYF4:Yb,Er, NaYF4:Yb,Er@NaGdF4 (UCNPs) and the UV–vis absorption spectrum of mitoxantrone (MX). (b) Fourier transform infrared spectra of UCMSNs (black line, I), UCMSNs modified amino group (red line, II) and anti-EpCAM antibody conjugated UCMSNs (blue line, UCMSNs-EpCAM, III). (c) Dynamic light scattering (DLS) size measurements of UCMSNs and UCMSNs-EpCAM dispersed in PBS for varied time durations (0-7 days). (d) Plots of T1 relaxation rate (R1) versus Gd3+ concentrations for UCMSNs in aqueous solution.

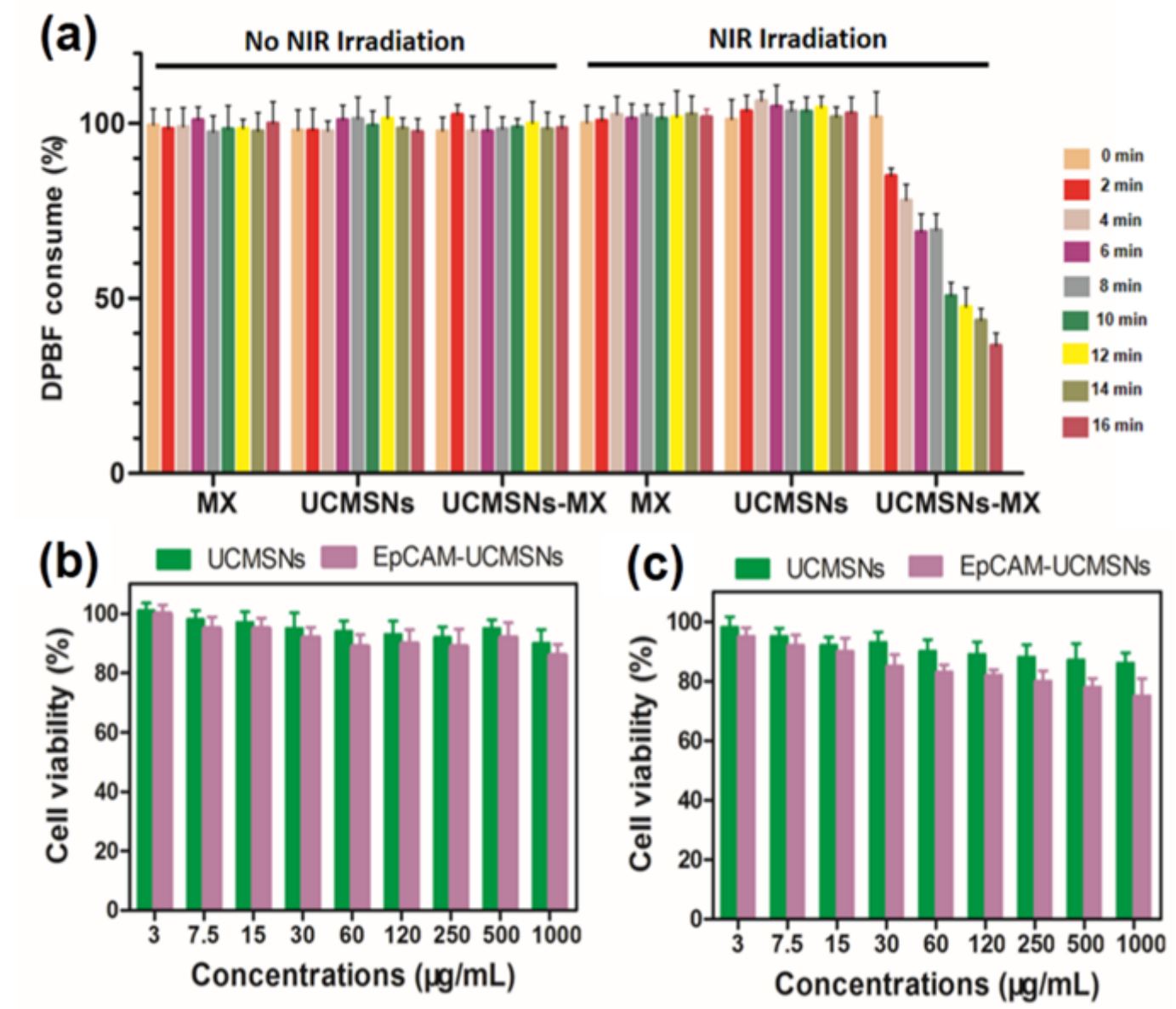

Figure 3

NIR-triggered singlet oxygen (1O2) generation under different time of NIR irradiation (a). In vitro toxicity evaluation of human pancreatic cancer BxPc-3 cells after co-incubation with UCMSNs/UCMSNs-EpCAM for 24 h (b) and 48 h (c) by Cell Counting Kit-8 (CCK-8) method.

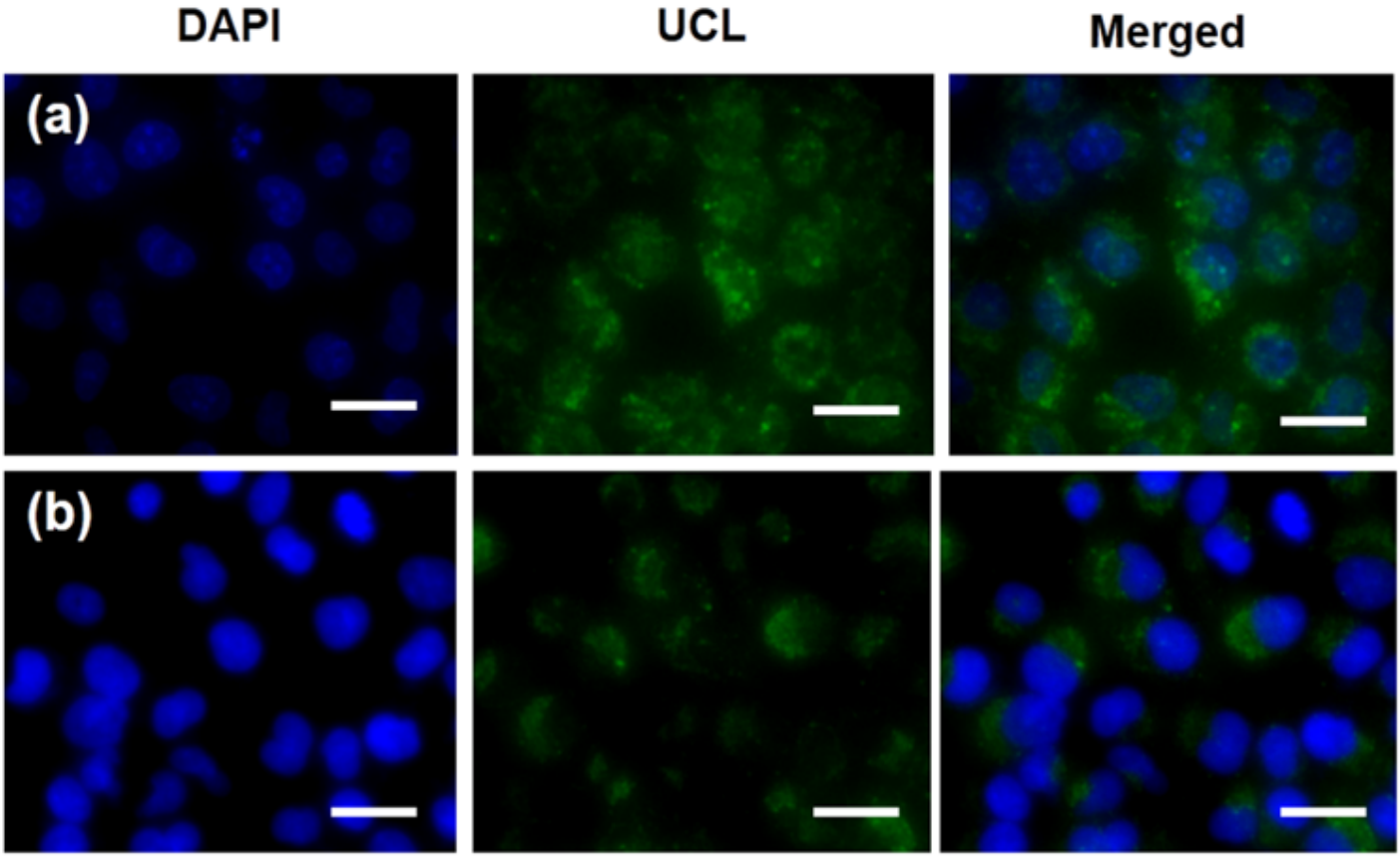

Figure 4

Confocal laser scanning microscopic (CLSM) imaging of BxPc-3 cells incubated with EpCAM-UCMSNs (a) and UCMSNs (b) for 4 h.

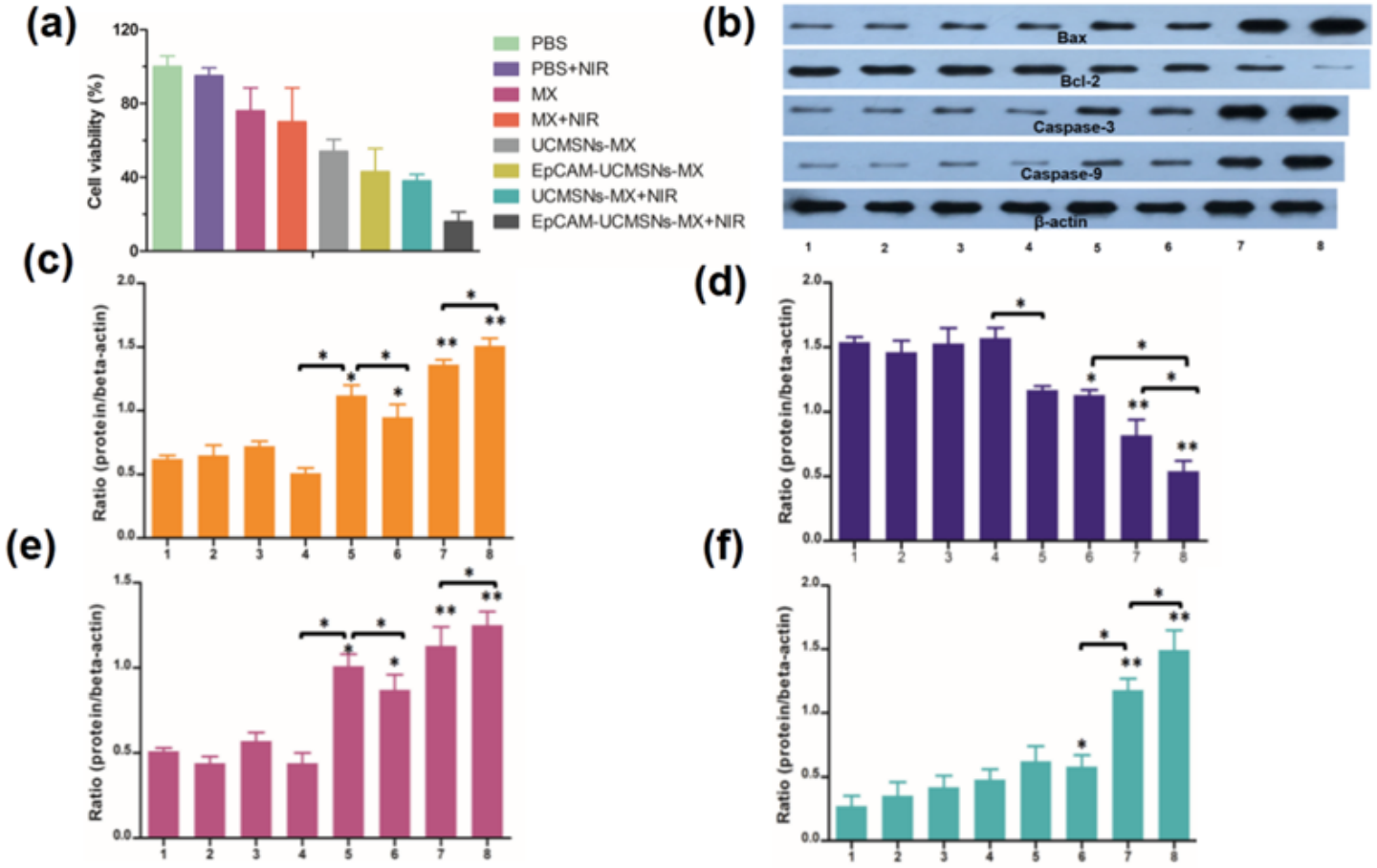

Figure 5

(a) The viability of BxPc-3 cells and (b) Western blot analyses of the expression of Bax (c), Bcl-2 (d), Caspase-3 (e) and Caspase-9 (f) protein after different treatments: (1) PBS (50 μL), (2) PBS (50 μL) lus NIR irradiation, (3) MX, (4) MX and NIR irradiation, (5) UCMSNs-MX solution, (6) EpCAM-UCMSNs-MX solution, (7) UCMSNs-MX solution and NIR irradiation, (8) EpCAM-UCMSNs-MX solution and NIR irradiation. Cells were irradiated with 980 nm laser at a power density of 320 mW/cm2 over a period of 5 min. [MX] = 0.5 μg/mL. *means $P < 0.05$, ** means $P < 0.01$.

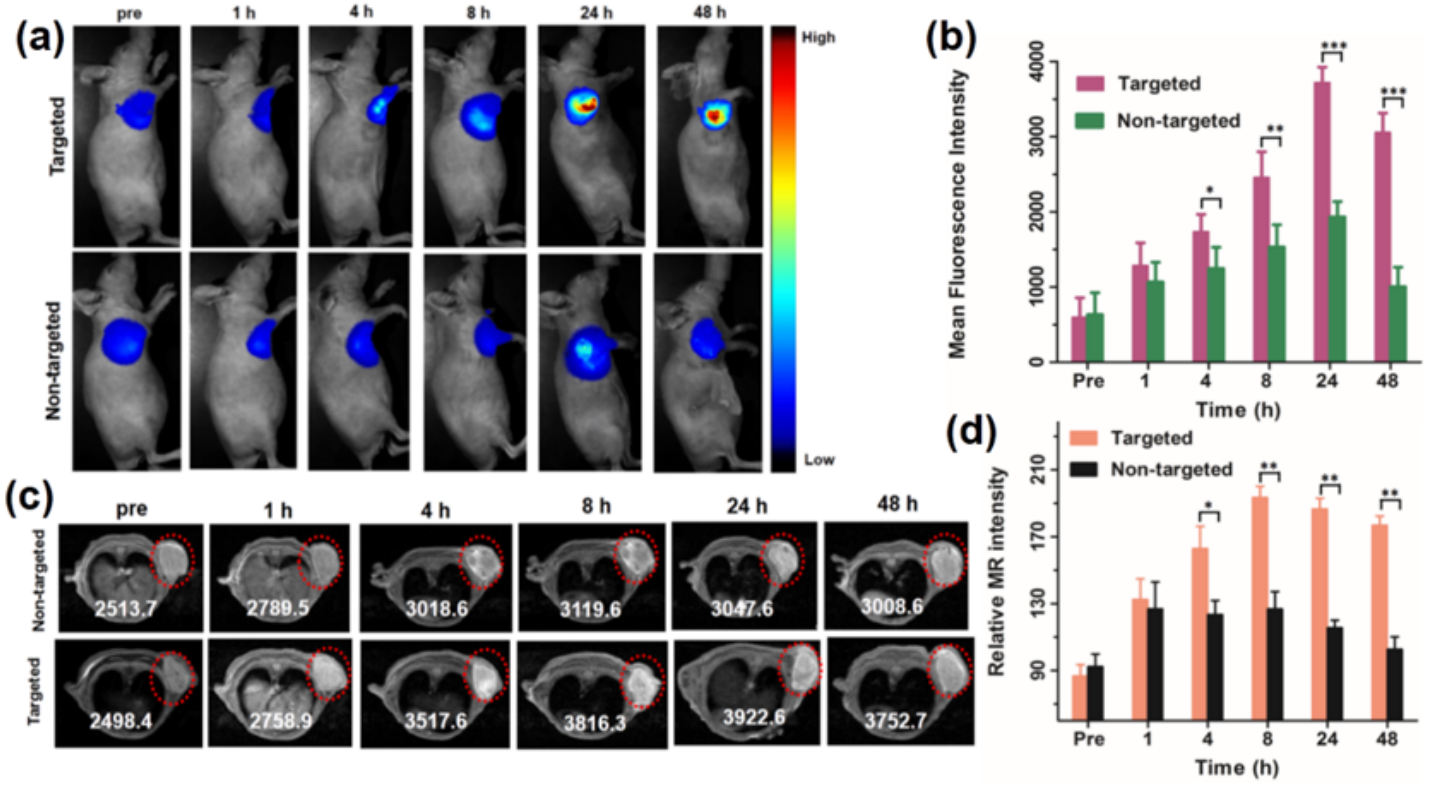

Figure 6

Targeted imaging experiments of EpCAM-UMSNs and UMSNs in vivo. (a) In vivo upconversion luminescence (UCL) images of BxPc-3 tumor-bearing mice obtained before and at different time points after intravenous injection of EpCAM-UMSNs (i.e., Targeted) and UMSNs (i.e., Non-targeted). (b) Comparison of the mean fluorescence intensities (MFI) between targeted and nontargeted groups at the different time points. (c) In vivo T1-MRI images of BxPc-3 tumor-bearing mice obtained before and at different time points after intravenous injection of EpCAM-UMSNs (i.e., Targeted) and UMSNs (i.e., Non-targeted) at designated time points (red dotted circles show the site of tumor). (d) Comparison of the relative MR intensities between targeted and non-targeted groups at the different time points. *means $P < 0.05$, ** means $P < 0.01$, *** means $P < 0.001$.

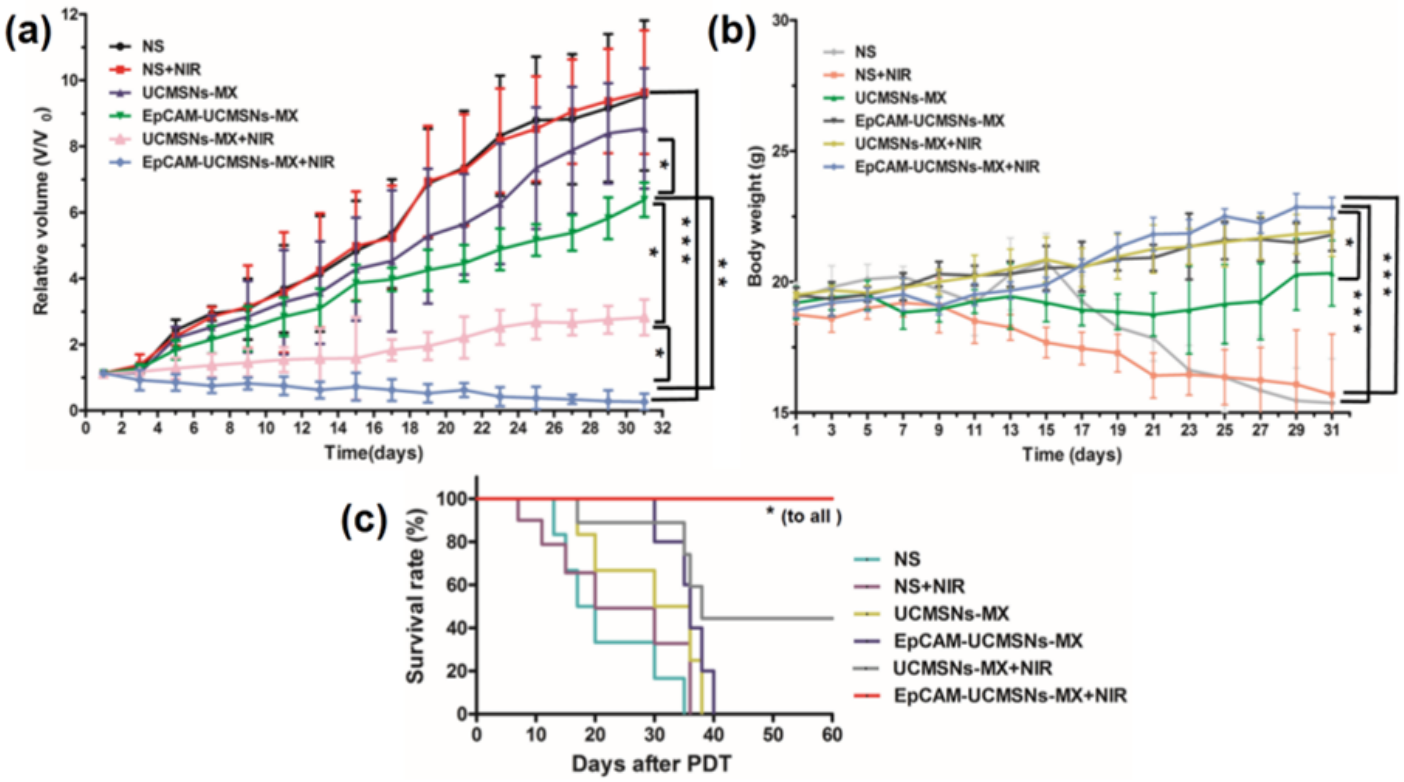

Figure 7

Tumor growth curves (a) and changes in body weight (b) of BxPc-3 tumor-bearing mice after the corresponding treatments over a period of a month. (c) Survival curves of BxPc-3 tumor-bearing mice in six groups with different treatments (n = 7 per group). *means $P < 0.05$, ** means $P < 0.01$, *** means $P < 0.001$.

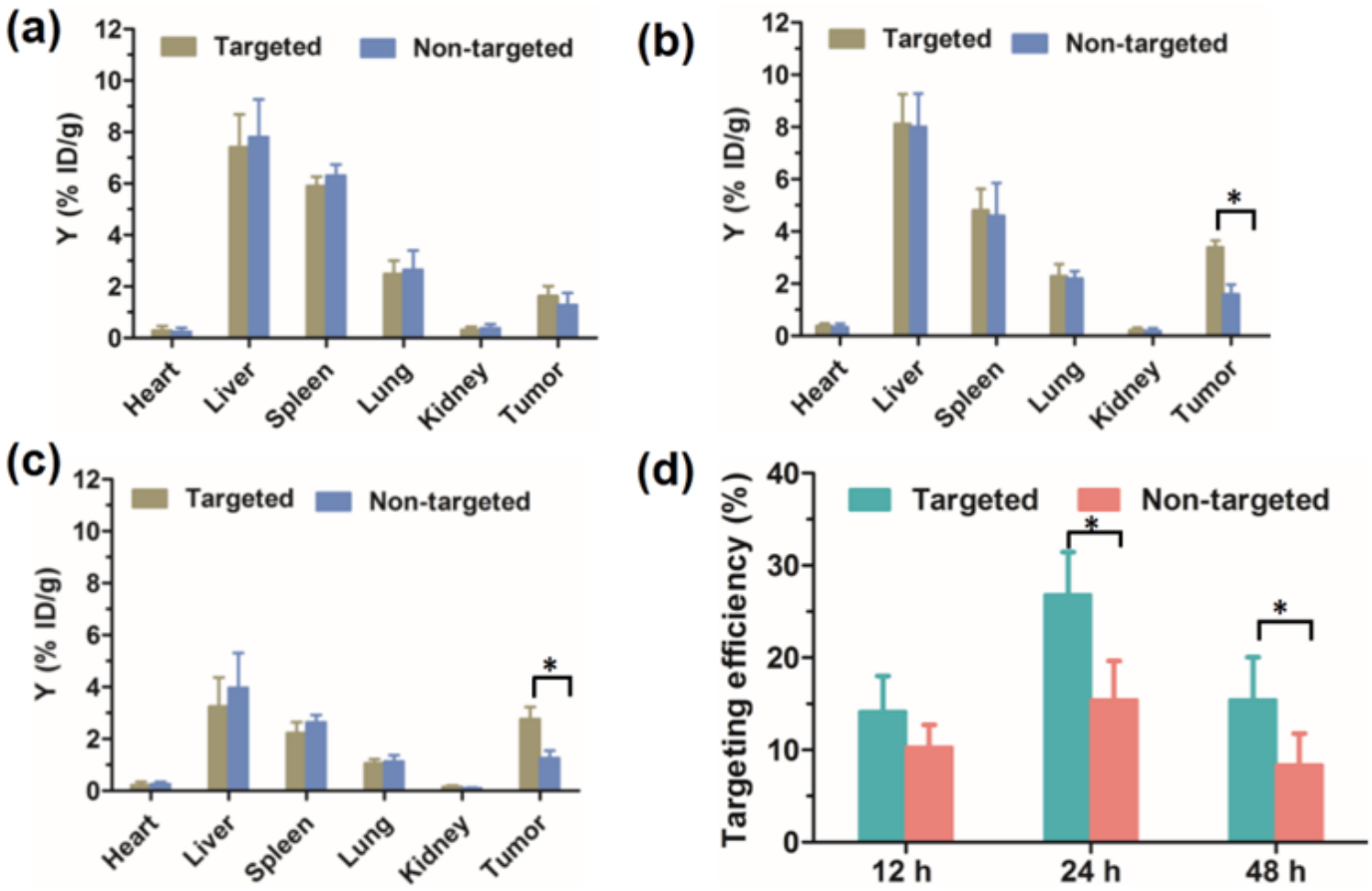

Figure 8

Biodistribution of EpCAM-UMSNs and UMSNs in mice post-injection. The concentration of Y element in the tumor and tissue samples was evaluated by ICP-MS at 12 h (a), 24 h (b), and 48 h (c) post-injection. (d) Targeting efficiency of EpCAM-UMSNs and UMSNs in mice at different time points post-injection. * means $P < 0.05$.

Supplementary Files

This is a list of supplementary files associated with this preprint. Click to download.

- Graphic.tif
- SupportingInformation.docx
- schema1.png